Journal of Translational Medicine

RESEARCH

Open Access

STAP2 promotes the progression of renal fibrosis via HSP27

Yuan Yuan[1†], Xiao Wei[1†], Xi Xiong[1†], Xiong Wang[2], Wei Jiang[3], Qihui Kuang[1], Kai Zhu[4], Chen Chen[5], Jingzheng Gan[5], Junjie Li[5], Jun Yang[6*], Lili Li[7*] and Pengcheng Luo[1*]

Abstract

Background Renal fibrosis is a key process in the progression from acute kidney injury (AKI) to chronic kidney disease (CKD), while the intricate mechanisms of renal fibrosis remain obscure. While the signal-transducing adaptor protein 2 (STAP2) was well-studied for its notable function in inflammation and immune-related disorders, its specific implication in renal fibrosis remains unclear. This study assessed the mechanism by which STAP2 could promote the progression of renal fibrosis.

Methods The expression level of STAP2 in fibrotic human samples, murine fibrosis models, and cellular fibrosis models was measured, respectively. Subsequently, immunoprecipitation (IP), mass spectrometry, and RNA sequencing (RNA-seq) were employed to identify HSP27 as an interacting protein and the PI3K-AKT signaling pathway. STAP2 was thereafter knocked down or overexpressed in both in vivo and in vitro models to assess the expression levels of pathway-related and fibrosis-related proteins. Finally, the important role of STAP2 in the fibrosis process in animal models induced by ischemia-reperfusion injury (IRI) and cisplatin was validated.

Results Functionally, in vivo assays demonstrated that the genetic knockout of STAP2 could remarkably mitigate epithelial-mesenchymal transition (EMT), diminish inflammatory cell infiltration, and reduce collagen deposition in mice with renal fibrosis. Conversely, in vitro assays employing STAP2-overexpressing cell models exacerbated the expression levels of fibrosis markers. The outcomes uncovered a potential mechanism by which STAP2 could modulate renal fibrosis through its impact on the expression level of phosphorylated HSP27, as well as modulating the PI3K/AKT signaling pathway.

Conclusions This comprehensive investigation delineated the noticeable function of STAP2 in the advancement of renal fibrosis, and the outcomes might contribute to the development of targeted therapies concentrated on STAP2 to mitigate renal fibrosis.

Keywords CKD, Renal fibrosis, STAP2, HSP27

[†]Yuan Yuan, Xiao Wei and Xi Xiong contributed equally to this work.

*Correspondence:
Jun Yang
735291410@qq.com
Lili Li
26061047@qq.com
Pengcheng Luo
pluo@whu.edu.cn
[1]Department of Urology, Wuhan Third Hospital and Tongren Hospital of Wuhan University, Wuhan 430060, China
[2]Department of Pharmacy, Wuhan Third Hospital, Wuhan 430060, China
[3]Department of Urology, Huangshi Central Hospital, Affiliated Hospital of Hubei Polytechnic University Huangshi, Huangshi 435000, China
[4]Department of Nephrology, Renmin Hospital of Wuhan University, Wuhan 430060, China
[5]School of Medicine, Wuhan University of Science and Technology, Wuhan 430060, China
[6]Department of Urology, Wuhan Third Hospital, Wuhan 430060, China
[7]Central Laboratory, Renmin Hospital of Wuhan University, Wuhan 430060, China

Introduction

Chronic kidney disease (CKD) is recognized by the progressive deterioration of renal function, accompanied by persistent inflammatory processes and the gradual onset of renal fibrosis, affecting nearly 10% of the global population, which constitutes a major public health concern [1, 2]. Fibrosis is a complex and dynamic process characterized by abnormal extracellular matrix deposition leading to scar formation, destruction of organ parenchyma, and loss of function. Renal interstitial fibrosis (RIF) is characterized by abnormal deposition of extracellular matrix (ECM) due to renal inflammation, oxidative stress, cell autophagy, and other factors. It represents the common final pathway for the progression of various renal diseases to end-stage kidney disease (ESRD) [3]. Tubular epithelial cells are critical targets in the progression of renal fibrosis, and their limited repair capacity makes them prone to epithelial-mesenchymal transition, senescence, apoptosis, and secretion of pro-inflammatory and pro-fibrotic factors after injury, thereby leading to renal fibrosis. The exact mechanism underlying the progression of renal fibrosis remains unclear, and the current therapies to slow down this progression are limited and nonspecific [4]. Once renal fibrosis occurs, it becomes irreversible; therefore, identifying novel therapeutic targets to intervene in this process could be a crucial step toward improving disease prognosis.

The signal-transducing adaptor protein (STAP) family, including STAP1 and STAP2, is a group of adaptor molecules involved in regulating multiple signaling pathways [5]. Previous studies have demonstrated that STAPs is expressed in various renal cells, such as tubular cells, glomerular cells, and fibroblasts. STAP2 expression level in tubular cells is significantly higher than that in other renal cells, accounting for approximately 70%. In tubular epithelial cells, which are primarily affected by renal injury, STAP2 is mainly localized in the cytoplasm. Both STAP1 and STAP2 possess a Pleckstrin homology domain at the N-terminus and a Src homology domain in the central region. STAP2, rather than STAP1, includes a proline-rich region and a YXXQ motif at the C-terminus [6], which may function as a potential binding site for signal transducer and activator of transcription 3 (STAT-3). Adaptor proteins interact with numerous intracellular signaling molecules, leading to alterations in their functions. Prior research has demonstrated that certain adaptor proteins can coordinate signaling pathways to achieve their functional effects, including cell migration, activation, proliferation, and differentiation [7]. With the advancement of research on STAP2, its functions are gradually elucidated. However, the function of STAP2 in renal fibrosis has not yet been documented.

This investigation was designed to figure out the intricate function of STAP2 in the context of renal fibrosis, aiming to transcending existing limitations in clinical treatment and laying a solid study for the discovery of novel therapeutic targets. We quantified the expression level of STAP2 in both human subjects with renal fibrosis and in murine models, subjected to unilateral ureteral obstruction (UUO), ischemia-reperfusion injury (IRI), and cisplatin (Cis) administration. Kidney fibrosis models were precisely established using STAP2 gene knockout mice in vivo and treating HK-2 cells with lipopolysaccharide (LPS) in vitro. Using these models, we found that STAP2 promoted the progression of renal fibrosis by activating the PI3K/AKT signaling pathway via regulating the phosphorylation of HSP27. This revealed the complex interactions of STAP2 in renal fibrosis progression, elucidated the intricate mechanisms underlying this pathology, and provided new insights for the prevention and targeted treatment of renal fibrosis.

Materials and methods

Human kidney samples

Human kidney samples ($n=8$) were collected from nephrectomy procedures conducted to address renal dysfunction triggered by ureteral stone obstruction (Supplementary Table 1). We obtained these kidney specimens from Wuhan Third Hospital and Huangshi Central Hospital. Normal control samples ($n=8$) were gathered from individuals with healthy kidneys who underwent nephrectomy due to either tumor-related or trauma-induced ruptured kidneys, without any concurrent kidney diseases. All procedures were performed adhering to the ethical principles outlined in the Helsinki Declaration. The Ethics Committee of Wuhan Third Hospital (WuSanYiLun KY2023-057) and Ethics Committee of Huangshi Central Hospital (2024-17) authorized these investigations. In this study, no form of compensation was provided to any human research participants.

STAP2 knockout mice and genotype

Breeding pairs of STAP2 null C57BL/6J mice (STAP2$^{-/-}$; age, 6-8-week) were purchased from Cyagen Biosciences Inc. that was headquartered in Suzhou (China) and subsequently housed in the Center of Experimental Animals at Wuhan Third Hospital. We maintain these mice particularly under specific pathogen-free conditions. For the induction of renal fibrosis models, male STAP-2$^{-/-}$ C57BL/6J mice (age, 8-10-week) were specifically utilized. Genotyping of these mice was carried out through genomic DNA extracted from their tails via polymerase chain reaction (PCR). The primer sequences employed for this genotyping procedure are accessible in Table 1. During genotyping, the presence of a singular 724 bp band was suggestive of the wild-type genotype, whereas the presence of only a 528 bp band signified the homozygous (STAP2$^{-/-}$) genotype. In the case of heterozygous

Table 1 PCR primers for mouse genotyping used in this study

Species	Gene	Forward primer (5′ to 3′)	Reverse primer (5′ to 3′)
Mouse	STAP2-KO	F1:TTGGCACAAGCATCTTAAGGAAGT	R1:GAGACTTCGAATCCCCTTCCTG
	STAP2-WT	F2:CTATGAGAAGGTTCTAGGTGTGTG	

Table 2 Primers for qRT-PCR used in this study

Species	Gene	Forward primer (5′ to 3′)	Reverse primer (5′ to 3′)
Human	STAP2	TGGCCCAGCTGTTGACTATG	AAAGACTTTGGGCTCTGGCT
	Col-I	GCCCTGCTGGTGCTCG	ACCCTGGGGACCTTCAGAG
	FN	AACCTTGCTCCTGACAGCTC	TTGGTGGGCTGACATTCTCC
Mouse	STAP2	GGTCTGAAAATCCGGGTGGC	GTAGTTCTGGGCTCCTTTCCAG
	Col-1	CGATGGATTCCCGTTCGAGT	GAGGCCTCGGTGGACATTAG
	FN	GGCCACCATTACTGGTCTGG	GGAAGGGTAACCAGTTGGGG

mice (STAP2$^{+/-}$), both the 724 and 528 bp bands were observed, as displayed in Supplementary Fig. 1A.

Animal models

We established murine models of renal fibrosis through three different methods: UUO, IRI, and cisplatin-induced renal interstitial fibrosis (RIF). For the UUO-induced RIF model, mice were anesthetized utilizing a face mask delivering 30% isoflurane. A right abdominal incision was made to expose the right ureter, which was either fully ligated 1 cm below the renal pelvis using 5.0 silk ligature (for 7 days ligated group) or manipulated without ligation (for the sham group). After 7 days, murine kidneys and serum were collected. In the IRI-induced RIF model, mice were anesthetized through a face mask delivering 30% isoflurane. The right kidney pedicle was exposed through a dorsal incision on the right side, and an atraumatic Schwartz micro-vessel clamp was applied to the right renal pedicle for 45 min. The removal of the clamp was subsequently performed to facilitate reperfusion, allowing the tissues to restore their normal coloration. Kidneys and serum were collected after 8 weeks. The cisplatin-induced RIF model involved injecting cisplatin at a dose of 8 mg/kg body weight four times (once a week). Kidneys and serum were collected on day 28.

Animals were divided into 4 groups randomly (n=6 per group): (1) wild-type sham-operated, (2) wild-type renal fibrosis, (3) STAP2$^{-/-}$ sham-operated, and (4) STAP2$^{-/-}$ renal fibrosis. These experiments were carried out adhering to the rules of Experimental Animal Ethics Committee of Wuhan Third Hospital (WuSanYiShiLun SY2023-003).

Cell cultivation and treatment

The China Center for Type Culture Collection (Wuhan, China) provided the normal human kidney proximal tubule epithelial cell line (HK-2), which was grown in a DMEM/F12 medium (#G4610-500ML, Servicebio, Wuhan, China) supplemented with 10% fetal bovine serum (FBS, Gibco, USA). Initially, we seeded HK-2 cells into six-well plates and allowed to incubate overnight in the complete medium. Subsequently, these cells underwent a transformative process with plasmids or siRNA particularly in the OPTI MEM medium (#Gnm22600-1, Genom, Zhejiang, China). Plasmids expressing Flag-tagged STAP2, HA-tagged HSP27 and siRNA were constructed by Gene Create (Wuhan, China). After a 24-hour incubation period, the cells were incubated in a complete medium supplemented with 10% FBS. To visualize the cells, a microscope was utilized, while the transfection rate was precisely indicated through the quantitative real-time transcription PCR (qRT-PCR) and Western blotting (WB). In an endeavor to simulate the in vitro assay of renal fibrosis, we seeded 1.5×10^6 cells into six-well plates, and the overnight incubation was performed in the complete medium. Following 12-hour starvation period without 10% FBS, we treated HK-2 cells (confluence, 60-70%) utilizing LPS (#L2880, Sigma, USA) at an ultimate concentration of 50 ng/ml. Subsequently, the cells were cultivated for additional assay after 24 h.

RNA isolation and qRT-PCR analysis

The process of isolating total RNA was performed using murine kidneys and HK-2 cells through a specialized RNA isolation kit (#R6934–01, Omega Bio-Tek, USA). Thereafter, we conducted cDNA synthesis employing the TOYOBO ReverTra Ace qPCR RT kit, adhering diligently to the protocols outlined by the manufacturer. After this intricate process, qRT-PCR was executed utilizing the Bio-Rad CFX Manager system. In this molecular investigation, indicators of fibrosis, involving collagen type I (Col-I) and fibronectin (FN), were precisely identified. The relative changes of mRNA level were determined by 2-△△ CT method with ACTB as control. The primer sequences utilized are accessible in Table 2.

Western blotting (WB)

Murine kidneys and HK-2 cells underwent lysis through lysis buffer, enriched with a protease inhibitor cocktail and phosphatase inhibitors, which were purchased from Servicebio. The quantification of protein content was performed through a BCA Protein Assay kit purchased from Servicebio. Subsequently, 20 μg of each protein specimen was precisely separated via 6%, 10%, or 12% SDS-PAGE, respectively, and the transfer particularly

onto polyvinylidene difluoride membranes was thereafter carried out. We blocked the membranes through 5% non-fat milk for a duration of 1 h, followed by an overnight incubation with a series of primary antibodies precisely detailed in Supplementary Table 2. This nocturnal incubation occurred at a temperature of 4 °C to ensure precision. The resulting blots were elegantly scanned utilizing a two-color infrared imaging system (Bio-Rad, USA) and subjected to analysis employing both ImageLab and ImageJ software, in which the latter was developed by the National Institutes of Health (Bethesda, USA).

Histology and immunohistochemistry assay

Paraffin-embedded murine renal sections, which cut at a thickness of four micrometers, underwent staining with hematoxylin-eosin (HE) on the basis of the instructions documented by the manufacturer. This precise process aimed to figure out the structural integrity of the kidney and fibrotic injuries. The extent of tubular injury was scored from 0 to 4 based on the percentage of the cortico-medullary region affected, as documented previously [8]: 0 indicating no damage, 1 for less than 25% damaged area, 2 for 25–50% damaged area, 3 for 50–75% damaged area, and 4 for more than 75% damaged area.

We investigated interstitial fibrosis and glomerulosclerosis through Masson staining, Sirius red staining, and immunohistochemistry targeting α-smooth muscle actin (α-SMA), FN, and Col-I in the renal tissue. The renal fibrotic-positive area was quantified by analyzing the percentage of colored pixels in the total field encompassing the cortico-medullary region. Six randomly selected fields were analyzed on each slide, specifically at 200× or 400× magnification.

We conducted histological and immunohistochemical (IHC) staining procedures adhering to protocols outlined by manufacturers in advance. Deparaffinizing each slide was performed, and antigen retrieval was thereafter executed. Once an overnight incubation was implemented with antibodies meticulously detailed in Supplementary Table 2 (temperature, four centigrade degree), each tissue specimen was subjected to incubation with a horseradish peroxidase-conjugated secondary antibody and subsequently stained using 3,3-diaminobenzidine tetrahydrochloride (DAB, #HP191902) purchased from Servicebio. Each slide's positive regions were captured under a TE2000-U microscope (Nikon Eclipse, Japan) at magnifications of 200× in six randomly selected fields. The analysis of resulting images was performed through ImageJ software.

Immunofluorescence staining

Frozen renal sections, precisely sliced at a 5-μm thickness, were dedicated to the subsequent staining of ECM-related proteins. We immersed these sections in a protein-blocking solution before undergoing a sequential incubation process with primary antibodies targeting Col-I (#GB11022-3), FN (#GB13091), and E-cadherin (E-ca) (#GB13083), which all purchased from Servicebio. Following this precise incubation, the treatment of sections was performed with appropriate secondary antibodies, accelerating the binding process. Additionally, 25 μL of DAPI solution was delicately applied to the samples and allowed to incubate for 5 min. Utilizing the capabilities of a fluorescence microscope equipped with a digital camera, the intricate patterns of fluorescence were precisely visualized.

To quantify the average fluorescence intensity, a rigorous analysis was performed through ImageJ software, and the average fluorescence intensity was computed through dividing the total fluorescence intensity of a specific region by its corresponding area. To ensure a comprehensive assessment, at least six distinct, non-overlapping regions were analyzed per sample.

Immunoprecipitation (IP) and mass spectrometry (MS) analysis

HK-2 cells underwent lysis utilizing the pre-cooled IP lysis buffer. Following centrifugation, the collection of resultants was performed, and overnight incubated separately with anti-FLAG (#F1804, Sigma) or anti-HA (#T0050, Affinity, China) antibodies particularly at a temperature of 4 °C. Concurrently, protein A/G-agarose beads were suspended in lysis buffer encompassing a protease inhibitor and left to being 4-hour incubated particularly at 4 °C. The rinsing of beads was conducted four times, and the expression levels of the eluted proteins were analyzed via WB.

For the comprehensive shotgun proteomic analysis of the eluted proteins, an initial step involved the partial separation of protein mixtures to approximately 1.5 cm using 10% SDS-PAGE. The region containing the proteins of the appropriate size was excised and subjected to in-gel tryptic digestion to extract peptides. These recovered peptides were thereafter analyzed through data-dependent liquid chromatography in conjunction with tandem mass spectrometry (MS/MS) on the Q Exactive™ liquid chromatography-mass spectrometry system attained from Thermo, USA.

In this intricate process, we injected peptide samples into an automatic sampler, followed by separation through a C18 trapping column (3 μm, 75 μm × 20 mm, 100 Å). Subsequently, they were eluted onto an analytical column (50 μm × 150 mm, 2 μm particle size, 100 Å pore size) attained from Thermo for further separation. The data acquisition encompassed the precise collection of both intact mass data from MS and fragmentation pattern data from MS/MS of the peptides. This was achieved through an advanced data-dependent acquisition (DDA)

strategy, incorporating dynamic exclusion techniques to enhance and maximize the depth of coverage.

The resulting data were thereafter subjected to identification through Protein Discoverer (V2.3), employing the Percolator algorithm. For this analysis, the UniProt human proteome reference database (uniprot-Human-20230111.fasta) served as the foundation. The results were filtered based on criteria with a cutoff value of ≥0.05 for Maximum Delta Cn and Maximum Rank for peptide-spectrum matches (PSMs), removing entries retrieved from the decoy database and contaminating proteins.

RNA sequencing (RNA-seq) analysis

Firstly, the total RNA from LPS-induced siNC or siSTAP2 HK-2 cells was extracted. Secondly using the Fragment Analyzer, RNA quality is accurately evaluated by generating a digital profile of RNA quality through RNA concentration measurement, 28 S/18S detection, and RIN/RQN assessment. Once qualified, we diluted the RNA to a concentration of 300 ng/μL for subsequent library preparation and sequencing, adhering precisely to instructions outlined by the manufacturer. Following sequencing, the sequencing data were filtered with SOAPnuke (v1.5.6) by: (1) removing reads containing sequencing adapter; (2) removing reads with more than 20% low-quality bases (base quality≤15); and (3) removing reads with over 5% unknown bases ('N'). Filtered reads were subsequently obtained and stored in FASTQ format. The aligning of sequenced reads was thereafter performed through HISAT2 (v2.1.0), and the resulting mapping data were converted and sorted utilizing Samtools (v1.4). The TPM value, computed by RSEM (v1.3.1), was utilized for precise quantification of gene expression level. To visualize the gene expression patterns across diverse samples, we plotted a heatmap through the pheatmap R package (v1.0.8). Subsequently, differential expression analysis was carried out via DESeq2 (v1.4.5) with a stringent significance threshold of Q value≤0.05 (or FDR≤0.001). For further functional insights, the clusterProfiler R package was used to perform enrichment analysis of the annotated differentially expressed genes using Gene Ontology (GO) and Kyoto Encyclopedia of Genes and Genomes (KEGG). With a strict criterion of Q value≤0.05, the pathways and enriched terms' significance levels were presented.

Protein-binding site prediction

Utilizing in silico methodologies, we identified putative functional domains modulating the interaction of STAP2 with HSP27. We retrieved AlphaFold PDB files STAP2_HUMAN (ID: AF-Q9UGK3-F1) and HSPB1_HUMAN (ID: AF-P04792-F1) from Uniprot to predict structures as receptor proteins and ligand proteins, respectively. Protein-protein docking was performed using HDOCK server to identify binding modes with the potential to mediate the interaction between STAP2 and HSPB1 [9]. Based on the Docking score and confidence score, the top 10 most probable binding models were developed. A greater negative docking score could be suggestive of an escalated probability of binding model. If the confidence score was higher than 0.7, it indicated that the probability of binding of the two molecules was high. If the confidence score was between 0.5 and 0.7, it was considered that the two molecules could bind together. If the confidence score was below 0.5, it indicated that the possibility of binding of two protein molecules was low (Supplementary Table 3). The top scoring model was analyzed for protein-ligand non-covalent associations via P LIP(https://projects.biotec.tu-dresden.de/plip-web/plip/index) [10].Structural visualizations were implemented using PyMOL 2.5.4 software.

Statistical analysis

We used ImageJ to quantify and standardize the results of WB, IHC, and IF and analyzed all data attained from independent assays through the GraphPad Prism software developed by GraphPad Software 8.0 (San Diego, CA). All data were expressed as mean±SEM (standard error of the mean). The examination of two groups was performed through the two-tailed Student's t-test, and multiple groups was performed through the one- or two-way analysis of variance (ANOVA) followed by Tukey's test. The linear relationship between the variables was represented by linear regression, while the coefficient (r) and P-value were evaluated using Spearman correlation analysis. For all studies, differences were considered significant at $P<0.05$.

Results

STAP2 was significantly upregulated in murine UUO kidneys and human fibrotic kidneys

Initially, we assessed the expression levels of STAP family members (STAP1 and STAP2) using the murine kidney transcriptome dataset GSE217650 [11]. In the dataset, a notable elevation particularly in the mRNA expression level of STAP2 was identified in the murine kidneys belonging to the UUO group relative to the sham group (Fig. 1A). We further confirmed this finding in another dataset GSE42303 (Fig. 1B). Subsequently, to investigate the changes of the expression level of STAP2 during advancement of renal fibrosis, we successfully established a UUO mouse model (Supplementary Fig. 2A). Relative to the sham group, mice in the UUO group exhibited significantly more severe tubular injury (Fig. 1C-D) along with a notable upregulation of fibrosis biomarkers, including α-SMA, Col-I, E-ca, and FN expression (Fig. 1C and E-G, Supplementary Fig. 2B, 2D-F). Furthermore, the

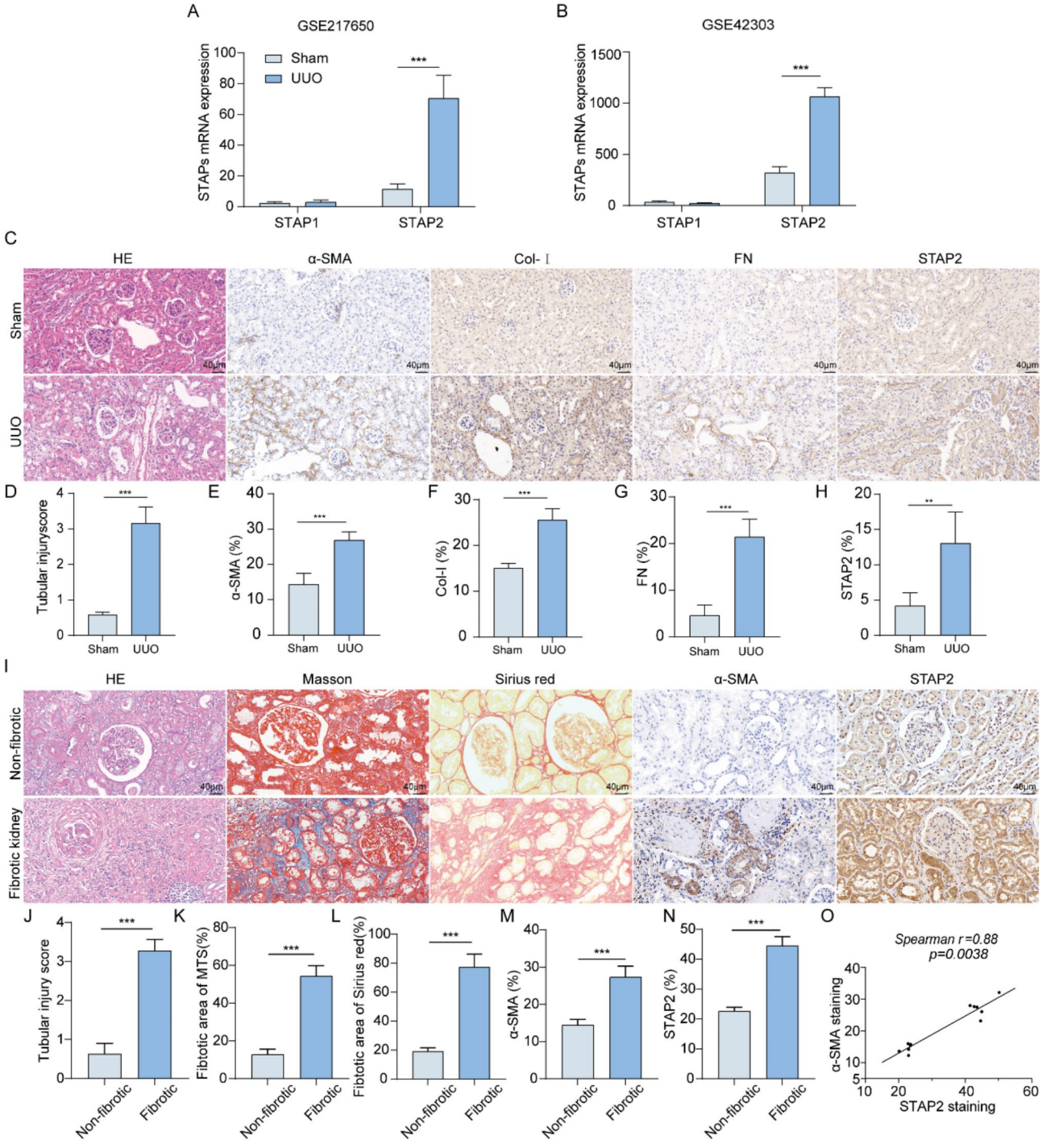

Fig. 1 STAP2 is significantly upregulated in fibrotic kidney. **(A**-**B)** Relative STAP1 and STAP2 mRNA levels in GSE217650 **(A)** and GSE42303 **(B)**, respectively. **(C**-**H)** Representative micrographs **(C)** and quantification of HE **(D)**, α-smooth muscle actin (α-SMA) **(E)**, Col-I **(F)**, FN **(G)** and STAP-2 **(H)** in sham and 7-day UUO mice. Magnification, 400×. Scale bar, 40 μm. $n = 6$ mice. **(I**-**N)** Representative micrographs **(I)** and quantitative analysis of HE **(J)**, Masson's staining **(K)**, Sirius red staining **(L)**, α-SMA **(M)** and STAP-2 **(N)** in human non-fibrotic and fibrotic kidney. Magnification, 400×. Scale bar, 40 μm. $n = 6$ patients. **(O)** Correlation between STAP2 expression level and the degree of α-SMA staining in all patients ($n = 8$). Error bars represent mean ± SEM. The comparable analysis of two groups was performed through two-tailed unpaired Student's t-test. $^{**}p < 0.01$, $^{***}p < 0.001$

significant escalation of STAP2 in the kidneys of UUO model mice was revalidated (Fig. 1C and H, Supplementary Fig. 2B-C). These results suggested the remarkable elevation of STAP2 expression particularly in the renal tissues of UUO mice.

Furthermore, compared with normal renal tissues, patients' fibrotic kidneys exhibited a marked interstitial fibrosis, as evidenced by histological analysis, encompassing HE staining, Masson's staining, and Sirius red staining (Fig. 1I-L). Additionally, a substantial elevation in STAP2 expression level was recorded in fibrotic kidneys, concomitant with an escalation of α-SMA expression level (Fig. 1I and M-N). Notably, Spearman correlation analysis unveiled a notable positive link of STAP2 level with α-SMA staining (r=0.88, P=0.0038) (Fig. 1O), reflecting a notable function of STAP2 in triggering the advancement of renal fibrosis.

Knockout of STAP2 attenuated renal fibrosis

To elucidate the function of STAP2 gene in the process of renal fibrosis, STAP2 knockout mice were generated to investigate whether deletion of STAP2 could alleviate UUO-induced renal fibrosis (Supplementary Fig. 1A-B). The kidneys in the UUO group exhibited a significantly thinner renal cortex relative to those in the sham group (Fig. 2A-B). In the UUO mouse model, knockout of STAP2 resulted in the noticeable alleviation of renal tubular dilation and inflammatory cell infiltration, moreover renal tubular injury scores, collagen deposition rates, and interstitial fibrosis areas were significantly attenuated. In the sham group, knockout of STAP2 showed no morphological abnormalities or changes in fibrotic areas (Fig. 2C-F). To determine whether STAP2 could exacerbate renal damage during renal fibrosis, we assessed ECM-related proteins in vivo. WB results revealed that in the UUO 7-day mouse model group, compared with the WT group, STAP2 knockout led to a significant decrease in the expression levels of fibrosis markers (FN and α-SMA), and a notable increase in E-ca protein expression level, significantly reducing the degree of renal fibrosis (Fig. 2G-J). Additionally, IHC results indicated that after STAP2 knockout in the UUO 7-day model group, the expression levels of FN, Col-I, and α-SMA proteins were significantly reduced, aligning with the WB results (Supplementary Fig. 3A-D). These outcomes demonstrated that the knockout of STAP2 could diminish the synthesis of ECM-related proteins in the kidneys of mice that were subjected to UUO, thereby mitigating the advancement of renal fibrosis.

STAP2 promoted the advancement of renal fibrosis in vitro

To demonstrate how STAP2 could regulate the function of renal tubular cells in the process of renal fibrosis, a fibrosis model was established in the human proximal tubular epithelial cell line (HK-2 cells) using LPS. The outcomes indicated that after 24 h of cell induction with different concentrations of LPS, the mRNA expression levels of STAP2, α-SMA, and FN peaked at 50 ng/ml (Supplementary Fig. 4A-C). According to the induction of cells with 50 ng/ml LPS at different time points, the protein expression level of STAP2 peaked at 24 h (Supplementary Fig. 4D-E). The outcomes unveiled an escalation in the expression levels of STAP2 and α-SMA protein after 24 h of induction with 50 ng/ml LPS (Fig. 3A-C). Subsequently, we selectively knocked down or overexpressed the STAP2 gene in the cell model, respectively. In the knockdown group without LPS treatment, the absence of significant difference in the protein expression levels of FN and α-SMA relative to the control group was noteworthy. However, the protein expression levels of FN and α-SMA in cells treated with LPS were significantly attenuated relative to the control group (Supplementary Fig. 4F, Fig. 3D-G). In comparison with the control group, the protein expression levels of FN and α-SMA were dramatically escalated in HK-2 cells overexpressing STAP2. Additionally, in LPS-treated cells, the expression levels of FN and α-SMA proteins were also significantly elevated in HK-2 cells overexpressing STAP2 compared with the control group (Supplementary Fig. 4G, Fig. 3H-K). These in vitro results emphasize that STAP2 may play a notable function in the renal fibrosis's pathogenesis.

STAP2 promoted the advancement of renal fibrosis through HSP27 in vitro

To identify downstream effector proteins of STAP2, immunoprecipitation (IP) and affinity-based mass spectrometry (MS) were performed on HK-2 cells to detect potential STAP2 binding partners. Following SDS-PAGE gel staining with Coomassie Brilliant Blue, interacting proteins were predominantly detected within the 25–35 kDa molecular weight range (Fig. 4A). Based on the MS results, we reviewed relevant literature and found that the HSP27 protein is located within the IP band range and plays an important role in renal fibrosis [12, 13]. Therefore, HSP27 was regarded as a downstream effector of STAP2. To further confirm the interaction between STAP2 and HSP27, immunofluorescence colocalization and co-immunoprecipitation (Co-IP) experiments were carried out. Immunofluorescence co-localization demonstrated that STAP2 and HSP27 were co-expressed in the cytoplasm. Co-IP experiments further confirmed the interaction between STAP2 and HSP27 proteins, and the interaction was significantly enhanced after overexpression of STAP2 or HSP27 (Fig. 4B-C). To validate the results, Alphabold2 Colab was employed to predict the binding sites between STAP2 and HSP27. The prediction outcomes identified HSP27 as a potential interacting protein of STAP2. STAP2 forms a

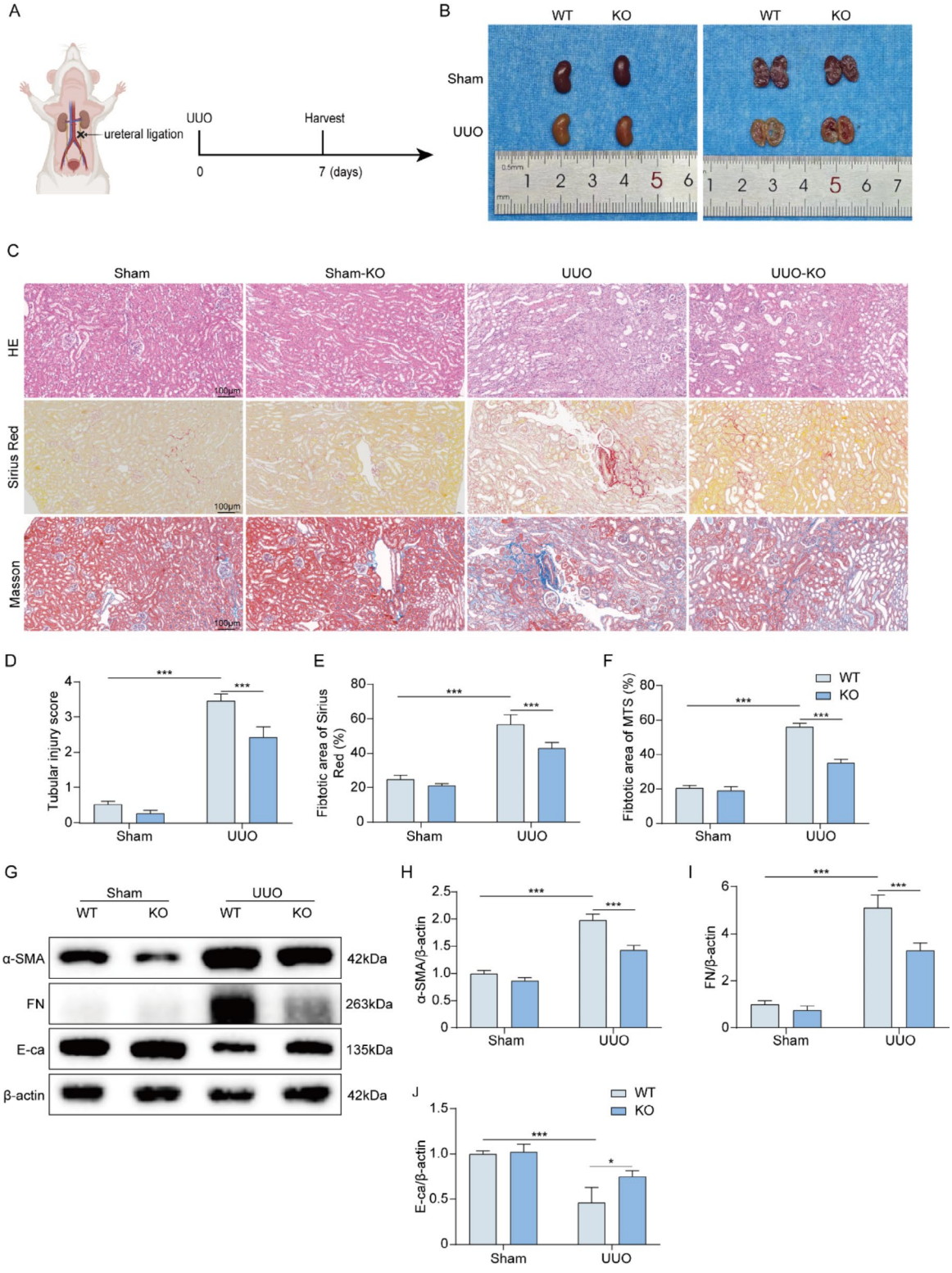

Fig. 2 Deletion of STAP2 alleviates UUO induced mouse renal fibrosis. **(A)** Scheme of the unilateral ureteral obstruction. **(B)** The gross appearance of kidneys from WT and STAP2-KO mice 7 days after UUO. **(C-F)** Representative micrographs and quantitative analysis of HE **(D)**, Sirius red staining **(E)** and Masson's staining **(F)** of WT and STAP2-KO murine kidneys with or without renal UUO. Magnification, 200×. Scale bar, 100 μm. $n = 6$ mice. **(G-J)** WB of α-smooth muscle actin (α-SMA) **(H)**, fibronectin (FN) **(I)** and E-cadherin (E-ca) **(J)** proteins in WT and STAP2-KO mice with or without UUO. $n = 6$ mice. Error bars represent mean ± SEM. The comparable analysis of multiple groups was performed through two-way ANOVA followed by Tukey's test. $^{*}p < 0.05$, $^{***}p < 0.001$

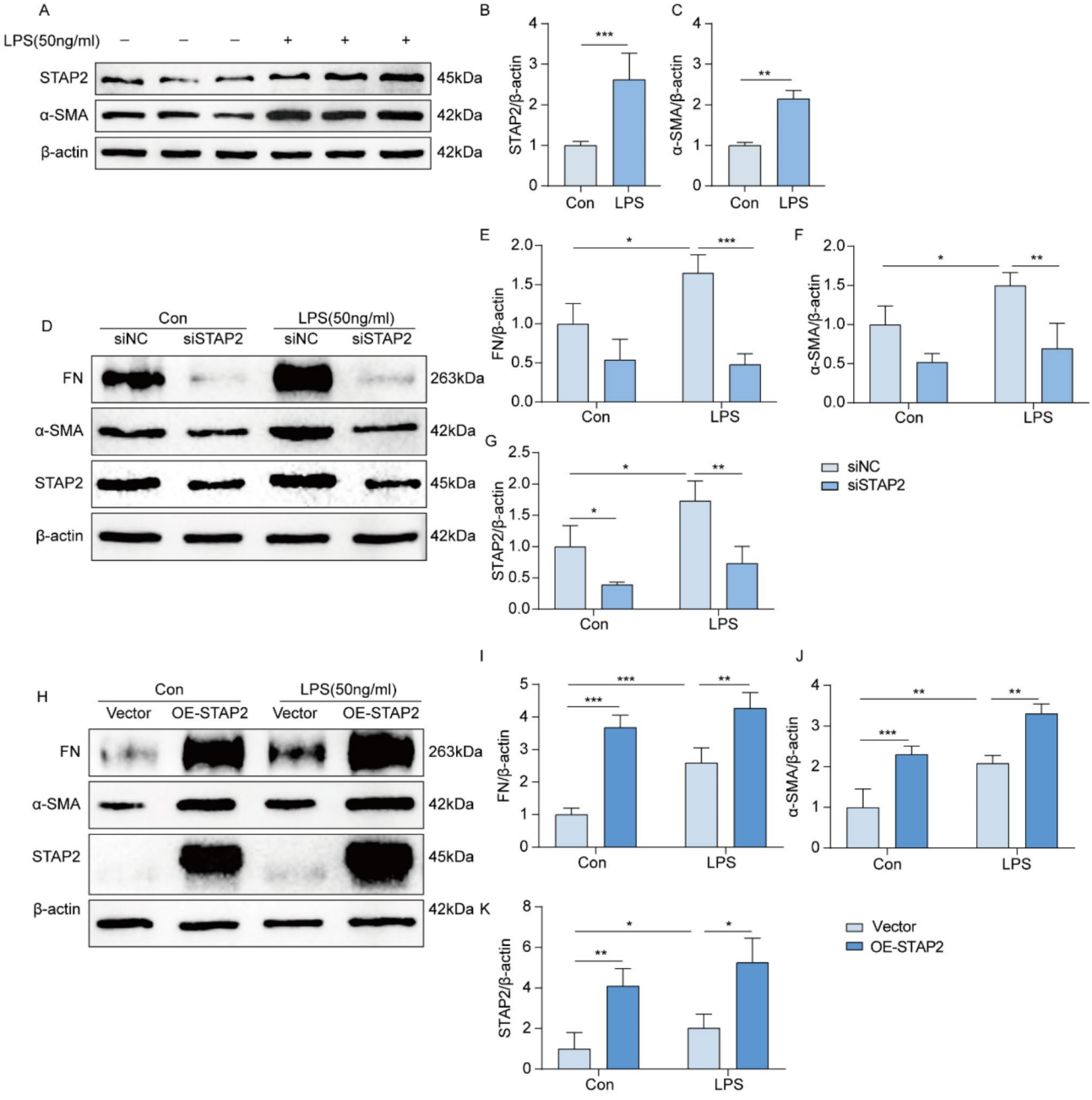

Fig. 3 STAP-2 promotes the advancement of renal fibrosis in HK-2 cell line. **(A-C)** WB of STAP-2 **(B)** and α-smooth muscle actin (α-SMA) **(C)** protein expression levels in HK-2 cells after treatment with LPS for 24 h. $n = 3$ samples. Error bars represent mean ± SEM. The comparable analysis of two groups was performed through two-tailed unpaired Student's t-test. **(D-G)** WB of FN **(E)**,α-SMA **(F)** and STAP2 **(G)** protein expression levels in NC siRNA (siNC) and STAP2 siRNA (siSTAP2) groups with or without LPS treatment. $n = 3$ samples. **(H-K)** WB of FN **(I)**, α-SMA **(J)** and STAP-2 **(K)** protein expression levels in Vector and overexpress STAP2 (OE-STAP2) groups with or without LPS treatment. $n = 3$ samples. Error bars represent mean ± SEM. The comparable analysis of multiple groups was performed through two-way ANOVA followed by Tukey's test. *$p < 0.05$; **$p < 0.01$; ***$p < 0.001$

hydrogen bond interaction network with the HSP27 protein. Protein interactions encompass multiple amino acid residues, such as Leu-245, Arg-56, and Asp-249 (Supplementary Fig. 5).

Next, it was attempted to explore whether knocking down HSP27 or using an HSP27 inhibitor could alleviate renal fibrosis induced by overexpression of STAP2. Initially, siRNA was utilized to knockdown HSP27 in HK-2 cells. A significant reduction of fibrosis biomarkers (α-SMA and FN) was noted, as well as a significant elevation in E-ca compared with the OE-STAP2 group (Fig. 4D, Supplementary Fig. 6A-C), indicating

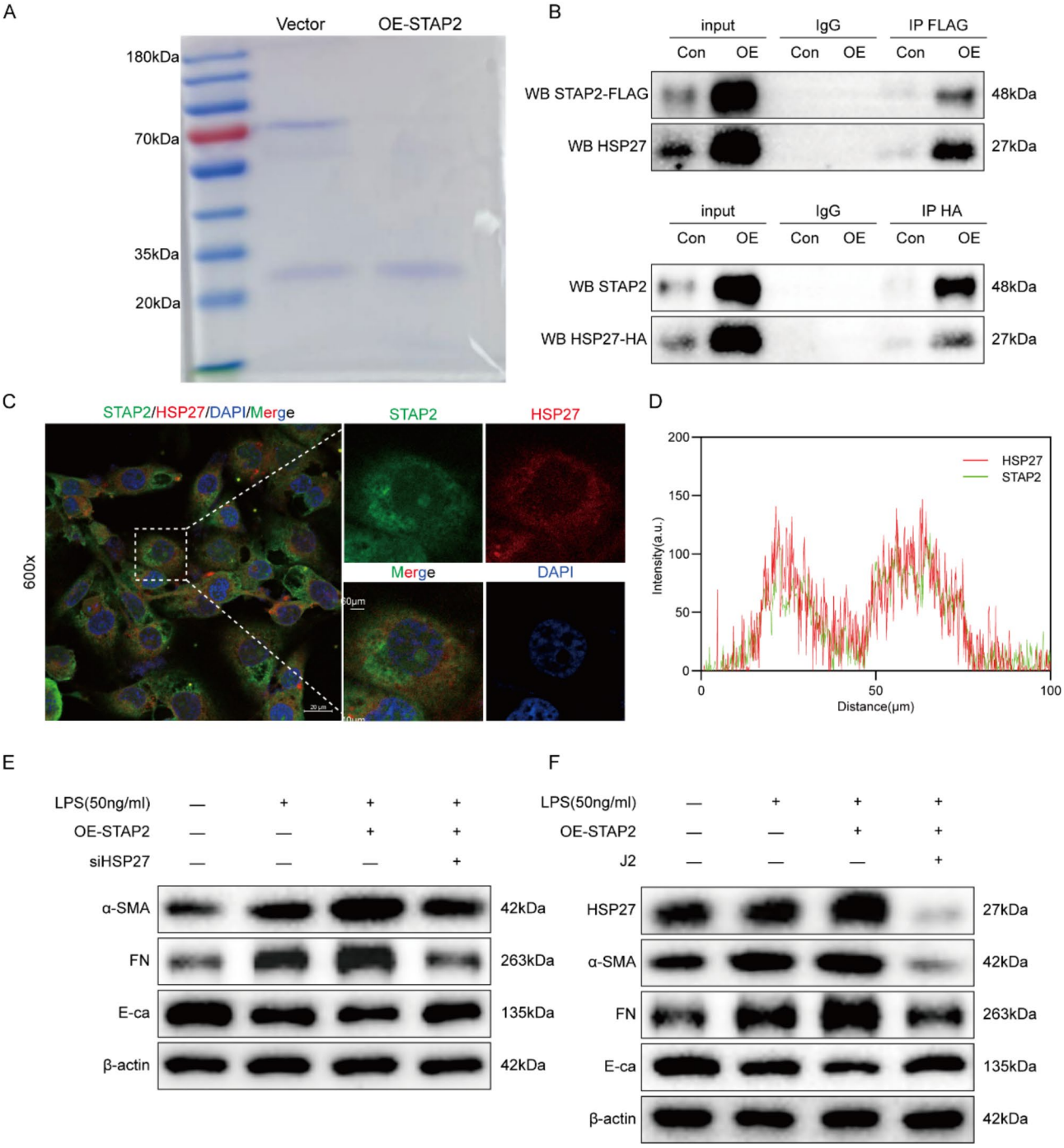

Fig. 4 STAP-2 regulates the advancement of renal fibrosis through HSP27 in vitro. **(A)** SDS-PAGE of Vector and overexpress STAP2 (OE-STAP2) in HK-2 cells, followed by Flag-pull down, and the sample was used for mass spectrometry (MS) for detection. **(B)** Co-immunoprecipitation of STAP2 and HSP27 in HK-2 cells was performed with overexpression of STAP2 and HSP27. **(C)** Colocalization analyses of STAP2 (green) with HSP27 (red). Magnification, 600 ×. Scale bar, 20 μm. $n = 3$ samples. **(D)** The distribution of STAP2 (green) or HSP27 (red) fluorescent intensity. **(E)** WB of the expression levels of α-smooth muscle actin (α-SMA), fibronectin (FN) and E-cadherin (E-ca) protein expression in OE-STAP2 and OE-STAP2 + siHSP27 groups with LPS treatment. $n = 3$ samples. **(F)** WB of the expression levels of HSP27, α-smooth muscle actin (α-SMA), fibronectin (FN) and E-cadherin (E-ca) protein expression in OE-STAP2 and OE-STAP2 + J2 groups with LPS treatment. $n = 3$ samples

a noticeable alleviation of renal fibrosis. Subsequently, these results were validated using immunofluorescence, which exhibited a remarkable reduction particularly in the expression levels of α-SMA and Col-I after knocking down HSP27 relative to the OE-STAP2 group (Supplementary Fig. 6D). Additionally, we inhibited the HSP27 by J2 and found that compared with the OE-STAP2 group, the addition of J2 resulted in a significant reduction particulrly in fibrosis markers (α-SMA and FN), and a significant escalation in E-ca (Fig. 4E, Supplementary Fig. 7A-D), indicating a marked alleviation of renal fibrosis. Subsequently, we validated these results, and relative to the OE-STAP2 group, the expression levels of α-SMA and Col-I significantly attenuated after inhibiting HSP27 with J2 (Supplementary Fig. 7E). Consequently, it can be demonstrated that STAP2 could modulate the advancement of renal fibrosis through HSP27 *in vitro*.

STAP2 modulated the advancement of renal fibrosis through the HSP27-PI3K/AKT axis

To identify the signaling pathways affected by STAP2 in promoting renal fibrosis and to reveal the specific mechanism of STAP2 in regulating renal fibrosis, the cells were divided into four groups (siNC, siSTAP2, LPS-siNC, and LPS-siSTAP2) for RNA-seq. The RNA-seq results revealed the differential gene expression after STAP2 gene knockdown (Supplementary Fig. 8A-B). The KEGG pathway annotation and enrichment analysis identified the PI3K/AKT signaling pathway (Fig. 5A-B).

A comprehensive analysis of the above results indicated that STAP2 could potentially influence the PI3K/AKT signaling pathway through HSP27, thereby regulating the process of renal fibrosis. To validate our findings, we treated HK-2 cells with LPS, followed by knockdown or overexpression of STAP2, respectively. As illustrated in Supplementary Fig. 8C-F, the protein levels of p-AKT, p-HSP27, and p-PI3K were diminished in the LPS-treated siSTAP2 group compared with the siNC group. Conversely, in the LPS-treated OE-STAP2 group, the expression levels of p-HSP27, p-PI3K, and p-AKT were dramatically elevated relative to the vector control group (Fig. 5C-F). To corroborate these findings at the tissue level, we detected protein in mouse kidney tissue, and observed a significant reduction particularly in the expression levels of p-HSP27, p-PI3K, and p-AKT in the UUO-KO group relative to the UUO-WT group (Fig. 5G-J). Additionally, other researchers have reported that activation of the PI3K/AKT signaling pathway could elevate the advancement of renal fibrosis in mice [14–16]. Consequently, STAP2 could modulate the advancement of renal fibrosis through the HSP27-PI3K/AKT axis.

STAP2 depended on the PI3K-AKT pathway to promote the advancement of renal fibrosis

To verify whether STAP2 would rely on the PI3K/AKT signaling pathway to promote the advancement of renal fibrosis, HK-2 cells were pretreated with the PI3K inhibitor LY294002. It was found that compared to the OE-STAP2 group, the addition of LY294002 attenuated the protein expression of p-AKT, as well as fibrosis markers (α-SMA and FN), and increased the protein expression of E-ca (Fig. 6A-F), indicating a noticeable alleviation of renal fibrosis. Similarly, to verify that HSP27 promotes renal fibrosis progression through the PI3K-AKT pathway, HK-2 cells were pretreated with the PI3K inhibitor LY294002. The results indicated that, compared with the OE-HSP27 group, inhibiting the PI3K/AKT pathway significantly reduced the expression level of fibrosis markers (α-SMA and FN), thereby alleviating renal fibrosis (Fig. 6G-K). Subsequently, these results were validated using immunofluorescence, which exhibited a remarkable reduction particularly in the expression levels of α-SMA and Col-I after inhibiting PI3K with LY294002 compared to the OE-STAP2 group (Fig. 6L). The outcomes indicated that in the HK-2 cell fibrosis model, STAP2 would depend on activation of the PI3K/AKT signaling pathway to promote the advancement of renal fibrosis.

Knockout of the STAP2 gene alleviated renal fibrosis progression following acute kidney injury (AKI) in mice

To further validate the function of the STAP2 gene in promoting the transition from AKI to CKD, mouse models induced by IRI and cisplatin were utilized. In the unilateral IRI 8-week model (Fig. 7A-B), the IRI-KO group exhibited dramatically lower renal tubular injury scores relative to the IRI-WT group, with fewer signs of tubular expansion, inflammatory cell infiltration, and collagen deposition (Fig. 7C, Supplementary Fig. 9B-C). Additionally, the expression levels of fibrosis markers (Col-I and α-SMA) were significantly attenuated (Supplementary Fig. 9A, 9D-E). Furthermore, the function of STAP2 in cisplatin-induced renal fibrosis was also investigated. Similarly, in the model of cisplatin-induced transition from AKI to CKD (Fig. 7D-E), the Cis-KO group exhibited a significantly attenuated renal tubular injury score compared to the Cis-WT group, with fewer signs of tubular expansion, inflammatory cell infiltration, and collagen deposition (Fig. 7F, Supplementary Fig. 9G-H). Additionally, the expression levels of fibrosis markers (α-SMA and Col-I) were significantly attenuated (Supplementary Fig. 9F, 9I-J). These data reconfirmed the notable function of STAP2 in promoting the transition from AKI to CKD and its significant involvement in the advancement of renal fibrosis.

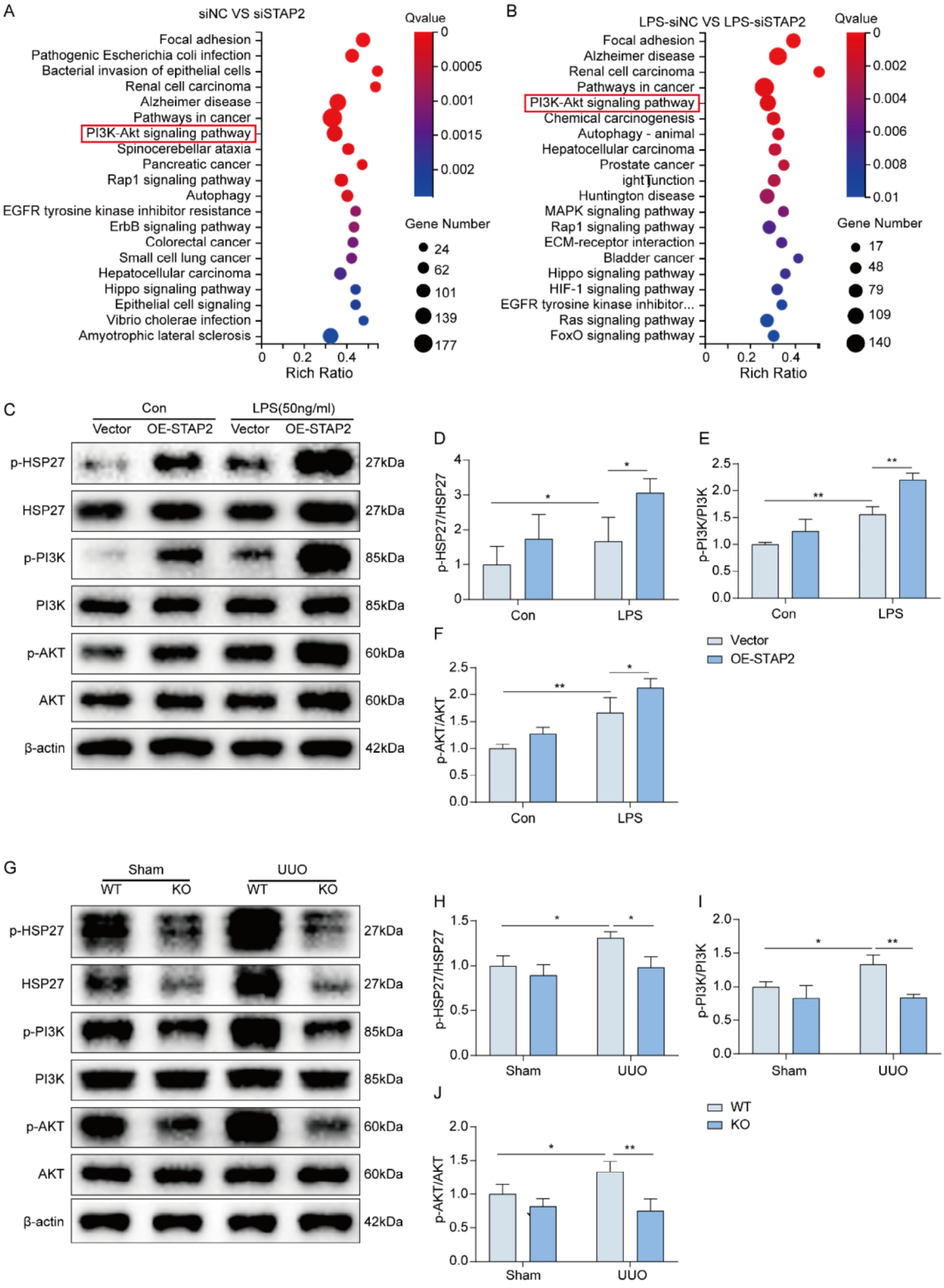

Fig. 5 STAP-2 regulates the advancement of renal fibrosis through HSP27-PI3K/AKT axis. **(A-B)** siNC vs. siSTAP2 **(A)** and LPS-siNC vs. LPS-siSTAP2 **(B)** KEGG pathway enrichment analysis of RNA-seq data. **(C-F)** WB **(C)** and quantification of p-HSP27/HSP27 **(D)**, p-PI3K/PI3K **(E)** and p-AKT/AKT **(F)** protein expression following overexpression of STAP2 with or without LPS treatment in vitro. $n = 3$ samples. **(G-J)** WB **(G)** and quantification of p-HSP27/HSP27 **(H)**, p-PI3K/PI3K **(I)** and p-AKT/AKT **(J)** protein expression in vivo. $n = 6$ mice. Error bars represent mean ± SEM. The comparable analysis of multiple groups was performed through two-way ANOVA followed by Tukey's test. $^{*}p < 0.05$; $^{**}p < 0.01$

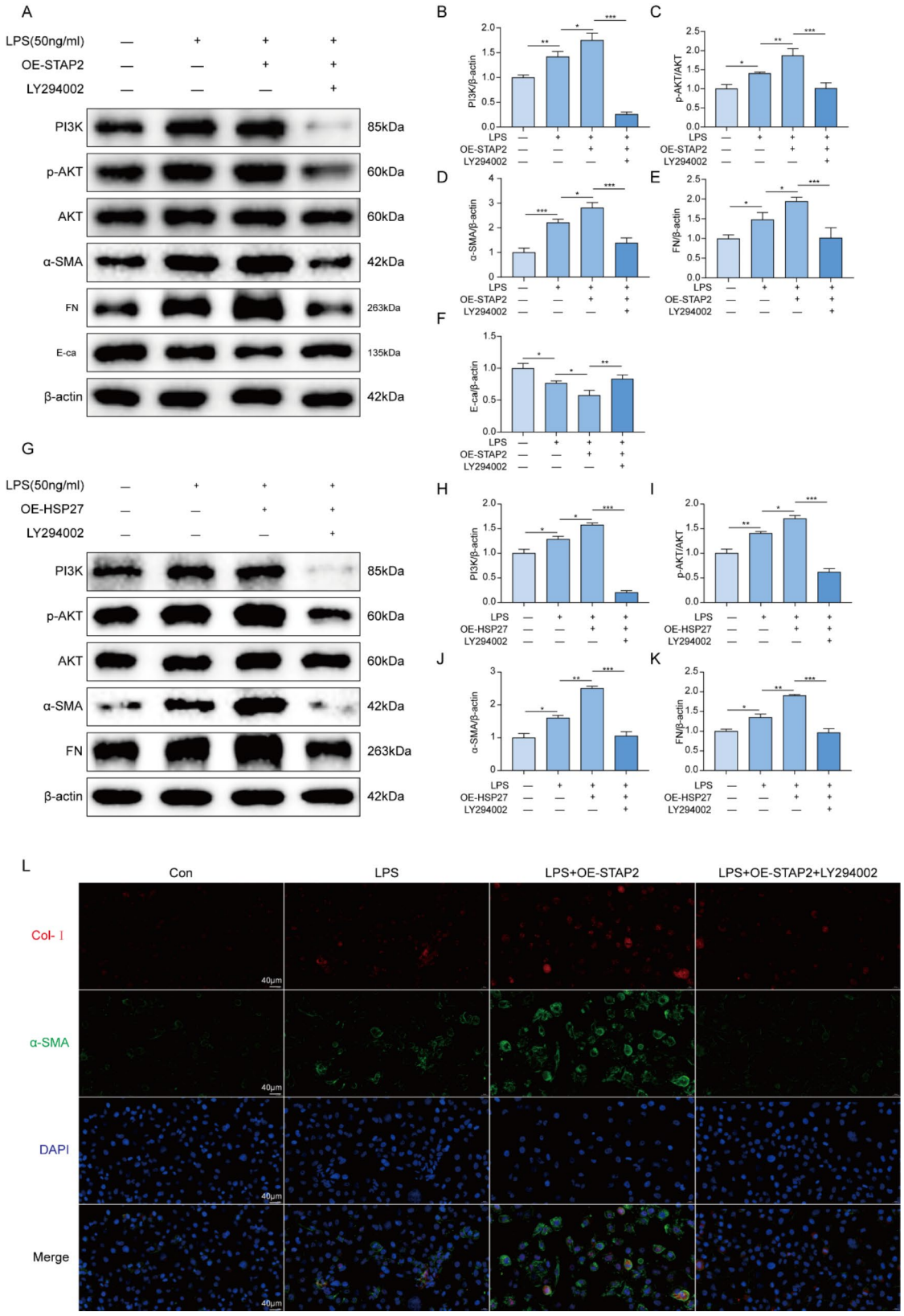

Fig. 6 (See legend on next page.)

(See figure on previous page.)

Fig. 6 Inhibition of PI3K alleviates STAP2 exacerbated renal fibrosis. **(A-F)** WB **(A)** and quantification of PI3K **(B)**, p-AKT/AKT **(C)**, α-smooth muscle actin (α-SMA) **(D)**, fibronectin (FN) **(E)**, and E-cadherin (E-ca) **(F)** protein expression levels in OE-STAP2 and OE-STAP2 + LY294002 groups with LPS treatment. $n = 3$ samples. Error bars represent mean ± SEM. The comparable analysis of multiple groups was performed through one-way ANOVA followed by Tukey's test. **(G-K)** WB **(G)** and quantifications of PI3K **(H)**, p-AKT/AKT **(I)**, α-smooth muscle actin (α-SMA) **(J)** and fibronectin (FN) **(K)** protein expression in OE-HSP27 and OE-HSP27 + LY294002 groups with LPS treatment. $n = 3$ samples. Error bars represent mean ± SEM. The comparable analysis of multiple groups was performed through one-way ANOVA followed by Tukey's test. **(L)** Representative micrographs of immunofluorescence staining of collagen type I (Col-I) and α-SMA expression levels in OE-STAP2 and OE-STAP2 + LY294002 groups with LPS treatment. $n = 3$ samples. *$p < 0.05$; **$p < 0.01$; ***$p < 0.001$

Discussion

This investigation, based on molecular plus experimental methods, was conducted at three levels: cellular, animal, and patients, and confirmed the key function of STAP2 in renal fibrosis resulting from various causes of kidney injury. The main outcomes of this investigation were summarized as follows: (1) a significant elevation in STAP2 expression level in kidney samples from fibrotic patients, as well as in mice subjected to UUO, IRI, or cisplatin treatment, and in LPS-stimulated HK-2 cells; (2) compared to the control group, the severity of renal injury and fibrotic markers significantly attenuated in STAP2 knockout mice and in HK-2 cells with STAP2 knockdown before LPS stimulation; (3) mechanistically, STAP2 could interact with HSP27 through a unique domain, promoting HSP27 phosphorylation and activation of the PI3K/AKT signaling pathway, effectively promoting the advancement of renal fibrosis.

STAP2 demonstrates a widespread expression pattern across various tissues and cell types in the human body, with particularly prominent presence in vital organs, encompassing the kidneys, intestines, and liver, as well as its ability to regulate multiple cellular events [17]. The function of STAP2 in organ fibrosis should be figured out, especially its function in renal fibrosis, which has never been documented. In our study, we demonstrated the upregulation of STAP2 in renal fibrosis tissue, as well as in the kidneys of mice subjected to UUO, IRI, and cisplatin treatment, and in the LPS-induced HK-2 cell model. The outcomes appeared consistent with those outlined previously, demonstrating that STAP2 promotes fibroblast generation, leading to scar formation in the skin [18].

This study concentrated on elucidating the mechanisms by which STAP2 could regulate the advancement of renal fibrosis. Prior studies have revealed the function of STAP2 in prostate cancer [19], breast cancer [20, 21], and various hematological malignancies [22, 23]. As research progresses, an increasing number of researchers are investigating non-tumor diseases, such as inflammatory bowel disease [24] and skin scar formation [18]. In the kidneys, STAP2 expression is mainly concentrated in the renal tubules, particularly in the epithelial cells of the renal tubules in fibrotic kidneys, which is consistent with the location affected by renal injury. STAP2 also plays a notable function in immune and inflammatory responses. STAP2 could modulate the expression and activity of STAT3, STAT5, and NF-κB [25]. In T cells, STAP2 could interact with FAK by recruiting E3-ubiquitin ligase c-Cb1, resulting in FAK degradation and altering cell adhesion to fibronectin [26]. STAP2 could modulate the chemotaxis of T cells induced by SDF-1α by activation of the Vav1/Rac1 signaling pathway [27]. STAP2 participates in AICD (activation-induced cell death) through direct interaction with caspase-8 and Fas1 [28]. In macrophages, STAP2 could directly interact with c-Fms, resulting in enhanced cell migratory capability [29, 30]. STAP2 may be a connector between MyD88 and IKK-α/β, upregulating the LPS/TLR4 signaling pathway and playing a crucial function in inflammatory responses [31].

This investigation identified HSP27 as an interacting protein and revealed that STAP2 regulated renal fibrosis via the PI3K/AKT signaling pathway, as determined through MS and RNA-seq. HSP27 is a molecular chaperone induced by chemical stimuli [32]. Previous research has reported that HSP27, a small heat shock protein with actin remodeling properties, not only functions as a molecular chaperone, but also mediates the EMT process in fibrosis, playing a notable function in activation of myofibroblasts in fibrosis [33]. Its function in fibrosis in the lungs, kidneys, and heart has also been well established [34, 35], confirming that HSP27 could be a primary mediator of renal fibrosis. The PI3K/AKT signaling pathway is widely present in cells and has a vital role in cell proliferation, differentiation, apoptosis, autophagy, invasion, migration, and EMT by responding to various signals [36]. The PI3K/AKT signaling pathway plays a notable function in renal injury by regulating the differentiation of fibroblasts and the deposition of EMT during the fibrosis process [15, 37–39]. The PI3K/AKT signaling pathway is recognized as one of the most important signaling pathways in renal fibrosis progression. The present investigation confirmed that dephosphorylated HSP27 could alleviate renal fibrosis caused by renal injury and inhibit the transition from AKI to CKD by inhibiting the phosphorylation of PI3K in the PI3K/AKT pathway. Overall, the outcomes indicated that STAP2 in the kidneys could regulate the process of renal fibrosis by modulating the PI3K/AKT signaling pathway via regulating HSP27 phosphorylation (Fig. 8).

The limitations of the present investigation are noteworthy. (1) This study confirmed that STAP2 promotes the phosphorylation of HSP27 to exert its function,

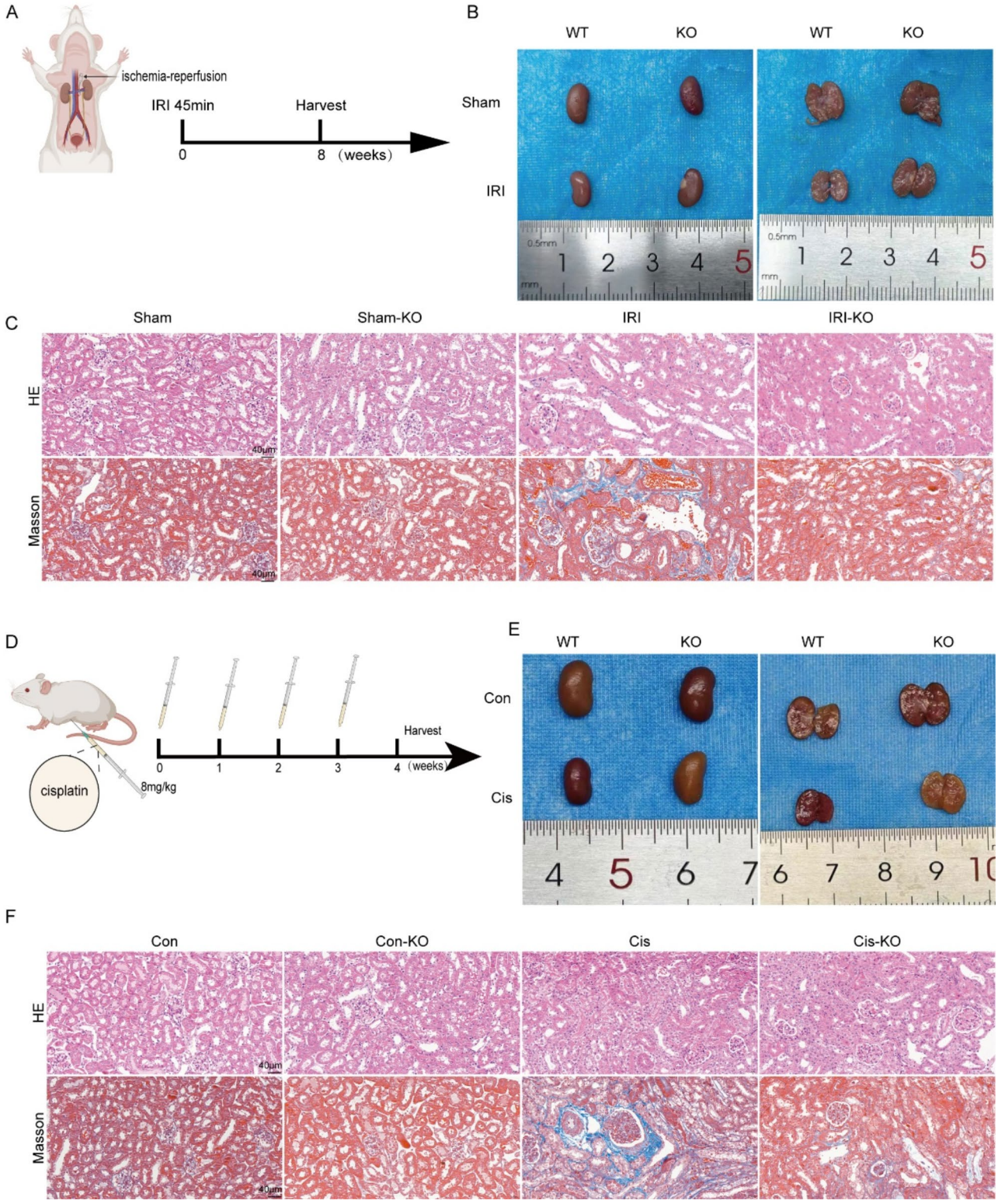

Fig. 7 Deletion of STAP2 alleviates IRI and cisplatin (Cis) induced mouse renal fibrosis. **(A)** Scheme of the ischemia-reperfusion injury. **(B)** The gross appearance of kidneys from WT and STAP2-KO mouse 8 weeks after IRI 45 min. **(C)** Representative micrographs of HE and Masson's staining of WT and STAP2-KO kidneys with or without IRI. Magnification, 400×. Scale bar, 40 μm. $n = 6$ mice. **(D)** Scheme of cisplatin-induced mouse renal fibrosis. **(E)** The gross appearance of kidneys from WT and STAP2-KO mouse after inject cisplatin once a week for 4 times. **(F)** Representative micrographs of HE, Masson's staining of WT and STAP2-KO kidneys with or without inject cisplatin. Magnification, 400×. Scale bar, 40 μm. $n = 6$ mice

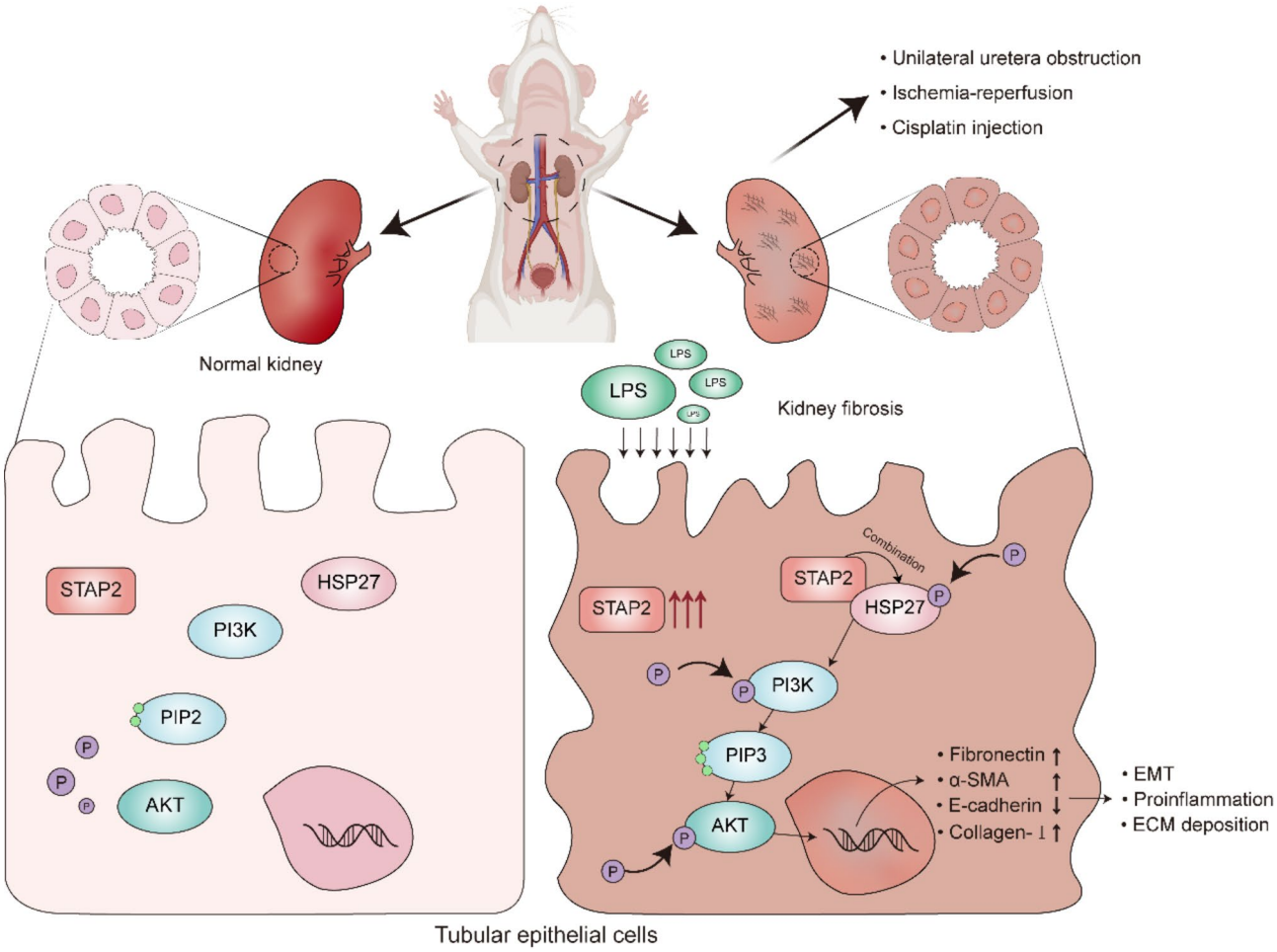

Fig. 8 STAP2 regulates the advancement of renal fibrosis through the HSP27-PI3K/AKT signaling pathway. After various factors lead to renal injury, the upregulation of STAP2 promotes the interaction between STAP2 and HSP27, further enhancing the phosphorylation of HSP27 and activation of the PI3K/AKT signaling pathway, which results in the loss of epithelial phenotype in epithelial cells, activation of fibroblasts and ultimately results in renal interstitial fibrosis

whereas the specific domain of STAP2 and the exact phosphorylation sites of HSP27 remain unclear. (2) Previous reports have found that with extended UUO modeling in mice (more than 10 days), HSP27 can exert anti-inflammatory and anti-apoptotic effects. In this study, this phenomenon was not observed in mice 7 days post-UUO, which requires further investigation. (3) The research was limited to HK-2 cells, and other immune cells, such as macrophages and T cells, have never been studied. (4) In addition to activation of PI3K/AKT signaling pathway, STAP2 might also participate in other signaling pathways, requiring further exploration. (5) The development of specific targeted drugs for STAP2 remains to be discovered.

Conclusions

In summary, this investigation identified the promoting function of STAP2 in renal fibrosis and revealed that the advancement of renal fibrosis by STAP2 could rely on its regulatory influence on the HSP27-PI3K/AKT pathway. An innovative therapeutic approach for treating renal fibrosis may involve targeting STAP2.

Abbreviations

ESRD	End-stage kidney disease
STAP2	Signal-transducing adaptor protein 2
EMT	Epithelial-mesenchymal transition
RIF	Renal interstitial fibrosis
UUO	Unilateral ureteral obstruction
Cis	Cisplatin
IRI	Ischemia-reperfusion injury
qRT-PCR	Quantitative real-time transcription PCR
RNA-seq	RNA sequencing
LPS	Lipopolysaccharide
Col-I	Collagen type I
α-SMA	α-smooth muscle actin
FN	Fibronectin
E-ca	E-cadherin
HE	Hematoxylin-eosin
IHC	Immunohistochemical
IP	Immunoprecipitation
MS	Mass spectrometry
WB	Western blotting

GO	Gene Ontology
KEGG	Kyoto Encyclopedia of Genes and Genomes

Supplementary Information

The online version contains supplementary material available at https://doi.org/10.1186/s12967-024-05776-6.

Supplementary Material 1

Supplementary Material 2

Supplementary Material 3

Acknowledgements
Thanks to the National Key R&D Program of China, Hubei Leading Talent Program in Medicine and Wuhan Application Foundation and Frontier Project for their financial support of this study.

Author contributions
Pengcheng Luo, Lili Li, Jun Yang and Xiong Wang were in charge of managing the study's overall design. Yuan Yuan, Xiao Wei, Qihui Kuang performed experiments. Junjie Li, Jingzheng Gan and Chen Chen conducted mouse breeding. Wei Jiang and Kai Zhu collected clinical samples and conducted clinical research. Yuan Yuan, Xiao Wei and Xi Xiong wrote the manuscript. Lili Li and Yuan Yuan modified the manuscript. The final draft had been read and amended by all authors.

Funding
This study was supported by National Key R&D Program of China (No. 2023YFC3605500, 2023YFC3605502), Hubei Leading Talent Program in Medicine and Wuhan Application Foundation and Frontier Project (No. 2020020601012209).

Data availability
Upon reasonable request, the corresponding author will make the study's data public.

Declarations

Ethical approval
Animal experiments were approved by Experimental Animal Ethics Committee of Wuhan Third Hospital (WuSanYiShiLun SY2023-003). Collected clinical samples and conducted clinical research were approved by Ethics Committee of Wuhan Third Hospital (WuSanYiLun KY2023-057) and Ethics Committee of Huangshi Central Hospital (2024-17).

Conflict of interest
The authors confirmed the absence of conflict of interest.

Received: 29 April 2024 / Accepted: 18 October 2024
Published online: 12 November 2024

References

1. Webster AC, et al. Chronic Kidney Disease Lancet. 2017;389(10075):1238–52.
2. Eckardt KU, et al. Evolving importance of kidney disease: from subspecialty to global health burden. Lancet. 2013;382(9887):158–69.
3. Gajjala PR, Sanati M, Jankowski J. Cellular and Molecular mechanisms of chronic kidney disease with diabetes Mellitus and Cardiovascular diseases as its comorbidities. Front Immunol. 2015;6:340.
4. Humphreys BD. Mechanisms of Renal Fibrosis. Annu Rev Physiol. 2018;80:309–26.
5. Matsuda T, Oritani K. STAP-2 adaptor protein regulates multiple steps of Immune and inflammatory responses. Biol Pharm Bull. 2021;44(7):895–901.
6. Minoguchi M, et al. STAP-2/BKS, an adaptor/docking protein, modulates STAT3 activation in acute-phase response through its YXXQ motif. J Biol Chem. 2003;278(13):11182–9.
7. Jordan MS, Singer AL, Koretzky GA. Adaptors as central mediators of signal transduction in immune cells. Nat Immunol. 2003;4(2):110–6.
8. Yang K, et al. Diosmetin protects against ischemia/reperfusion-induced acute kidney injury in mice. J Surg Res. 2017;214:69–78.
9. Yan Y, et al. The HDOCK server for integrated protein-protein docking. Nat Protoc. 2020;15(5):1829–52.
10. Salentin S, et al. PLIP: fully automated protein-ligand interaction profiler. Nucleic Acids Res. 2015;43(W1):W443–7.
11. Yuan Y, et al. Novel targets in renal fibrosis based on bioinformatic analysis. Front Genet. 2022;13:1046854.
12. Li J, et al. ERK and p38 MAPK inhibition controls NF-E2 degradation and profibrotic signaling in renal proximal tubule cells. Life Sci. 2021;287:120092.
13. Wang X, et al. Salt-induced phosphoproteomic changes in the subfornical organ in rats with chronic kidney disease. Ren Fail. 2023;45(1):2171886.
14. Wang Z, et al. Curcumin attenuates renal interstitial fibrosis of obstructive nephropathy by suppressing epithelial-mesenchymal transition through inhibition of the TLR4/NF-κB and PI3K/AKT signalling pathways. Pharm Biol. 2020;58(1):828–37.
15. Li R, et al. Fufang Shenhua tablet inhibits renal fibrosis by inhibiting PI3K/AKT. Phytomedicine. 2023;116:154873.
16. Zhang Y, et al. Signaling pathways involved in Diabetic Renal Fibrosis. Front Cell Dev Biol. 2021;9:696542.
17. Kashiwakura JI, Oritani K, Matsuda T. The functional properties and physiological roles of Signal-Transducing adaptor Protein-2 in the Pathogenesis of Inflammatory and Immune disorders. Biomedicines, 2022. 10(12).
18. Zhou Q, et al. KGF-2 regulates STAP-2-Mediated Signal Transducer and activator of transcription 3 signaling and reduces skin scar formation. J Invest Dermatol. 2022;142(7):2003. –2013.e5.
19. Kitai Y, et al. STAP-2 protein promotes prostate cancer growth by enhancing epidermal growth factor receptor stabilization. J Biol Chem. 2017;292(47):19392–9.
20. Ang HL, et al. Putting the BRK on breast cancer: from molecular target to therapeutics. Theranostics. 2021;11(3):1115–28.
21. Ikeda O, et al. Interactions of STAP-2 with brk and STAT3 participate in cell growth of human breast cancer cells. J Biol Chem. 2010;285(49):38093–103.
22. Wolfe HR, Rein LAM. The Evolving Landscape of Frontline Therapy in Chronic Phase Chronic Myeloid Leukemia (CML). Curr Hematol Malig Rep. 2021;16(5):448–54.
23. Sekine Y, et al. STAP-2 interacts with and modulates BCR-ABL-mediated tumorigenesis. Oncogene. 2012;31(40):4384–96.
24. Fujita N, et al. Signal-transducing adaptor protein-2 regulates macrophage migration into inflammatory sites during dextran sodium sulfate induced colitis. Eur J Immunol. 2014;44(6):1791–801.
25. Sekine Y. [Novel adaptor protein, STAP-2 functions as a signal modulator in immune system]. Yakugaku Zasshi. 2010;130(6):769–75.
26. Sekine Y, et al. Signal-transducing adaptor protein-2 regulates integrin-mediated T cell adhesion through protein degradation of focal adhesion kinase. J Immunol. 2007;179(4):2397–407.
27. Sekine Y, et al. Signal-transducing adaptor protein-2 regulates stromal cell-derived factor-1 alpha-induced chemotaxis in T cells. J Immunol. 2009;183(12):7966–74.
28. Sekine Y, et al. Signal-transducing adaptor protein-2 modulates Fas-mediated T cell apoptosis by interacting with caspase-8. J Immunol. 2012;188(12):6194–204.
29. Ikeda O, et al. STAP-2 regulates c-Fms/M-CSF receptor signaling in murine macrophage raw 264.7 cells. Biochem Biophys Res Commun. 2007;358(3):931–7.
30. Ikeda O, et al. Enhanced c-Fms/M-CSF receptor signaling and wound-healing process in bone marrow-derived macrophages of signal-transducing adaptor protein-2 (STAP-2) deficient mice. Biol Pharm Bull. 2008;31(9):1790–3.
31. Sekine Y, et al. Modulation of TLR4 signaling by a novel adaptor protein signal-transducing adaptor protein-2 in macrophages. J Immunol. 2006;176(1):380–9.
32. Alderson TR, et al. Local unfolding of the HSP27 monomer regulates chaperone activity. Nat Commun. 2019;10(1):1068.
33. Vidyasagar A, et al. HSP27 is involved in the pathogenesis of kidney tubulointerstitial fibrosis. Am J Physiol Ren Physiol. 2008;295(3):F707–16.
34. Yoo YJ, et al. Drug like HSP27 cross linkers with chromenone structure ameliorates pulmonary fibrosis. Front Pharmacol. 2023;14:1203033.
35. Hazra J, Vijayakumar A, Mahapatra NR. Emerging role of heat shock proteins in cardiovascular diseases. Adv Protein Chem Struct Biol. 2023;134:271–306.

36. Zhu FQ, et al. Curcumin suppresses Epithelial-Mesenchymal Transition of Renal Tubular Epithelial Cells through the inhibition of Akt/mTOR pathway. Biol Pharm Bull. 2017;40(1):17–24.
37. Du YM, et al. Effect of bradykinin on rats with thromboangiitis obliterans through PI3K/Akt signaling pathway. Eur Rev Med Pharmacol Sci. 2019;23(22):10169–76.
38. Hsu HS, et al. Involvement of ER stress, PI3K/AKT activation, and lung fibroblast proliferation in bleomycin-induced pulmonary fibrosis. Sci Rep. 2017;7(1):14272.
39. Li D, et al. Hydroxychloroquine alleviates renal interstitial fibrosis by inhibiting the PI3K/Akt signaling pathway. Biochem Biophys Res Commun. 2022;610:154–61.

Publisher's note